Interatomic potential for the Cu-Ta system and its application to surface wetting and dewetting

Adham Hashibon,[1,2,*] Alexander Y. Lozovoi,[3] Yuri Mishin,[4] Christian Elsässer,[1,2] and Peter Gumbsch[1,2]
[1]*Fraunhofer-Institut für Werkstoffmechanik IWM, Wöhlerstraße 11, 79108 Freiburg, Germany*
[2]*Institut für Zuverlässigkeit von Bauteilen und Systemen, Universität Karlsruhe (TH), Kaiserstraße 12, 76131 Karlsruhe, Germany*
[3]*Atomistic Simulation Centre, School of Mathematics and Physics, Queen's University of Belfast, Belfast, BT7 1NN Northern Ireland, United Kingdom*
[4]*Department of Physics and Astronomy, MSN 3F3, George Mason University, Fairfax, Virginia 22030, USA*
(Received 26 December 2007; published 25 March 2008)

An angle-dependent interatomic potential has been developed for the Cu-Ta system by crossing two existing potentials for pure Cu and Ta. The cross-interaction functions have been fitted to first-principles data generated in this work. The potential has been extensively tested against first-principles energies not included in the fitting database and applied to molecular dynamics simulations of wetting and dewetting of Cu on Ta. We find that a Cu film placed on a Ta (110) surface dewets from it, forming a Cu droplet on top of a stable Cu monolayer. We also observe that a drop of liquid Cu placed on a clean Ta (110) surface spreads over it as a stable monolayer, while the extra Cu atoms remain in the drop. The stability of a Cu monolayer and instability of thicker Cu films are consistent with recent experiments and first-principles calculations. This agreement demonstrates the utility of the potential for atomistic simulations of Cu-Ta interfaces.

DOI: 10.1103/PhysRevB.77.094131 PACS number(s): 34.20.Cf, 68.08.Bc, 31.15.xv, 68.60.−p

I. INTRODUCTION

Interfaces between different phases are of significant fundamental interest and play an important role in many areas of technology. This is particularly true for interfaces between highly dissimilar phases of very different chemical composition and atomic structure. In this work, the Cu-Ta system studied is a good example of such dissimilar phases, since Cu and Ta have practically zero mutual solid solubility, have different crystal structures (fcc Cu versus bcc Ta), as well as highly different melting temperatures, mechanical strength, chemical reactivity, and many other properties. The Cu-Ta system is also relevant to microelectronic systems, since Ta thin films can be used as diffusion barriers separating Cu conductor lines from the semiconductor (e.g., Si) substrate in integrated circuits.[1–4]

It is well recognized that large-scale atomistic simulations can give new insights into many material phenomena, particularly occurring at interfaces. A major impediment to their broader application is the lack of reliable interatomic potentials for many materials. Most of the existing interatomic potentials for metallic systems are based on the embedded-atom method (EAM).[5] While accurate EAM potentials have been developed for a few fcc metals (see, e.g., Ref. 6 for a review), the method is less reliable for bcc metals in which the interatomic forces include an angle-dependent component. The challenge becomes even greater when dealing with binary systems in which one or both of the main phases are bcc. Although EAM potentials have recently been constructed and applied to simulations of Cu-Ta interfaces,[7–9] a more reliable description of bonding in this highly disparate system involving a bcc metal requires a model reaching beyond the regular EAM formalism.

The goal of this paper is to develop an angle-dependent interatomic potential for the Cu-Ta system and to verify its applicability to Cu-Ta interfaces. We choose the functional form of the recently proposed *angular-dependent potential* (ADP) method[10] and utilize the existing potentials for pure Cu and Ta.[11,12] Given that the experimental Cu-Ta phase diagram[13] contains no intermediate solid phases, we fit the cross-interaction functions to first-principles data only. To enhance the transferability of the potential to interface simulations, the fitting and testing data include a number of layered crystal structures as well as energy-separation curves for coherent Cu-Ta interfaces.

The potential generation and testing procedures and results are presented in Sec. II. In Sec. III, we apply the potential to atomistic simulations of wetting and dewetting of Cu from a Ta substrate. We show that the results of these simulations are well consistent with recent experimental data and first-principles calculations,[14] which confirms the suitability of the potential for atomistic studies of Cu-Ta interfaces.

II. INTERATOMIC POTENTIAL FOR THE CU-TA SYSTEM

A. Angular-dependent potential method

To account for the covalent component of bonding in the Cu-Ta system, we apply the ADP method as proposed earlier for the Fe-Ni system.[10] In the ADP method, the total energy E_{tot} is written in the form

$$E_{tot} = \frac{1}{2}\sum_{i,j(j\neq i)} \Phi_{s_i s_j}(r_{ij}) + \sum_i F_{s_i}(\bar{\rho}_i) + \frac{1}{2}\sum_{i,\alpha} (\mu_i^\alpha)^2 + \frac{1}{2}\sum_{i,\alpha,\beta} (\lambda_i^{\alpha\beta})^2 - \frac{1}{6}\sum_i \nu_i^2, \quad (1)$$

where the Roman indices i and j refer to atoms and the Greek superscripts to Cartesian directions. The first two terms in Eq. (1) represent pair interactions between the atoms and their embedding energies, respectively. Together they constitute the functional form of the regular EAM potential.[5]

The pair-interaction potential $\Phi_{s_i s_j}(r_{ij})$ depends only on the scalar distance r_{ij} between atoms i and j and on their chemical species s_i and s_j. The embedding energy F_{s_i} is a function of the host electron density $\bar{\rho}_i$ induced on atom i by all other atoms of the system,

$$\bar{\rho}_i = \sum_{j \neq i} \rho_{s_j}(r_{ij}), \tag{2}$$

where the electron density $\rho_{s_j}(r)$ assigned to atom j is a function of the scalar distance r_{ij}. Note that the first two terms in Eq. (1) have central-force character, i.e., do not depend on angles between interatomic bonds.

The noncentral character of the bonding is represented by the rest of the terms in Eq. (1), which depend on dipole vectors,

$$\mu_i^{\alpha} = \sum_{j \neq i} u_{s_i s_j}(r_{ij}) r_{ij}^{\alpha}, \tag{3}$$

and quadrupole tensors,

$$\lambda_i^{\alpha\beta} = \sum_{j \neq i} w_{s_i s_j}(r_{ij}) r_{ij}^{\alpha} r_{ij}^{\beta}, \tag{4}$$

ν_i being the trace of $\lambda_i^{\alpha\beta}$,

$$\nu_i = \sum_{\alpha} \lambda_i^{\alpha\alpha}. \tag{5}$$

In these expressions, $u_{ss'}(r)$ and $w_{ss'}(r)$ are the two additional pairwise functions introduced in the ADP method. The terms depend on angles between interatomic bonds and penalize the total energy for deviations of atomic environments from cubic symmetry. For example, they make contributions to E_{tot} when a cubic crystal is subject to nonhydrostatic strains, thus affecting the elastic constants. They also contribute to the formation energies of ordered compounds. The angular terms modify (generally, increase) the energy of lattice defects and can be especially important in atomically disordered alloys, amorphous solids, and liquids.

An ADP description of the binary system Cu-Ta requires 13 functions: $\Phi_{\mathrm{CuCu}}(r)$, $\Phi_{\mathrm{TaTa}}(r)$, $\Phi_{\mathrm{CuTa}}(r)$, $\rho_{\mathrm{Cu}}(r)$, $\rho_{\mathrm{Ta}}(r)$, $F_{\mathrm{Cu}}(\bar{\rho})$, $F_{\mathrm{Ta}}(\bar{\rho})$, $u_{\mathrm{CuCu}}(r)$, $u_{\mathrm{TaTa}}(r)$, $u_{\mathrm{CuTa}}(r)$, $w_{\mathrm{CuCu}}(r)$, $w_{\mathrm{TaTa}}(r)$, and $w_{\mathrm{CuTa}}(r)$. In this work, we employ the existing EAM potential for Cu (Ref. 11) and the recently developed ADP potential for Ta.[12] Since the Cu potential is based on the regular EAM formalism, the functions $u_{\mathrm{CuCu}}(r)$ and $w_{\mathrm{CuCu}}(r)$ are set to zero. With the given Cu and Ta potentials, we only need to construct the cross-interaction functions $\Phi_{\mathrm{CuTa}}(r)$, $u_{\mathrm{CuTa}}(r)$, and $w_{\mathrm{CuTa}}(r)$. The invariant transformation coefficients s_{Ta}, g_{Cu}, and g_{Ta} (see, e.g., Refs. 6 and 15 for their definition) are used as additional adjustable parameters.

B. Fitting and testing database

The database used for fitting and testing the Cu-Ta potential contains first-principles data only. For bulk crystal structures, such data have been generated by the plane-wave pseudopotential method as implemented in the CPMD program.[16] For the sake of consistency, we kept the calculation parameters as similar to those used for generating the ADP potential for pure Ta (Ref. 12) as possible. In brief, the calculations employ the local density approximation within the density-functional framework. The core states of Ta and Cu are represented by norm-conserving Troullier-Martins pseudopotentials, relativistic for Ta and nonrelativistic for Cu. The copper pseudopotential requires the plane-wave cutoff energy as high as 100 Ry, which is used throughout. The **k**-point sampling in all calculations is approximately equivalent to the $12\times12\times12$ Monkhorst-Pack grid in a $1\times1\times1$ cubic cell. A specific feature of the Cu-Ta system is an interplay between fcc- and bcc-based structures. To further reduce the errors arising from the numerical integration over the Brillouin zone, all energies are referred to those of pure components having the same lattice, whereas the fcc-bcc energy differences for pure Cu and Ta are separately evaluated to high precision. More details on the numerical setup can be found in Ref. 12.

The phase diagram of the Cu-Ta system practically shows zero mutual solid solubility between Cu and Ta and does not contain any intermetallic compounds or other solid phases.[13] We have, therefore, chosen to fit the potential to first-principles binding relations (energy versus atomic volume) for several artificial ordered compounds that do not exist in the phase diagram. Such compounds include $L1_2$-Cu_3Ta, $L1_0$-CuTa, $L1_1$-CuTa, $B2$-CuTa, and $L1_2$-Ta_3Cu.[17] They represent three different chemical compositions and different types of ordering on the fcc and bcc lattices, thus spanning a significant area of configuration space. In addition, a fcc supercell containing a stack of three Cu (111) layers followed by three Ta (111) layers has been constructed to represent coherent Cu-Ta interfaces. The formation energy ΔE of each crystal structure relative to the equilibrium fcc Cu and bcc Ta has been computed for several atomic volumes around the energy minimum. Note that these calculations do not include any relaxation with respect to relative dimensions of the supercells or any internal degrees of freedom.

Binding relations for a few other structures have also been computed but used only for testing the potential. They include artificial fcc-based layered structures containing stacking sequences of CuCuTa (111) and CuTaTa. Furthermore, considering that C11 compounds were found to have rather low energies in the Fe-Ni system,[10] their formation energies in the Cu-Ta system have also been computed for the Cu_2Ta and Ta_2Cu stoichiometries. The C11 structure can be thought of as formed from fcc by filling (002) layers in the sequence CuCuTaCuCuTa$\cdots$ (respectively, TaTaCuTaTaCu$\cdots$) and then allowing the c/a ratio to vary. The calculations have been performed for a set of c/a ratios with volume relaxation at each c/a. The function ΔE versus c/a thus obtained (which is similar to the Bain path of the fcc-bcc transformation) has two special points corresponding to the fcc- and bcc-based C11 structures, which are denoted as $C11_f$ and $C11_b$, respectively. Their energy has been additionally relaxed by allowing local atomic displacements (full relaxation). Finally, isolated substitutional impurities are represented by a $2\times2\times2$ (32 atoms) fcc Cu supercell with a single Ta impurity and a $3\times3\times3$ (54 atoms) bcc Ta supercell with a single Cu impurity. In both cases, full relaxation of the supercell has been implemented and the impurity solubility energy has been computed relative to the equilibrium fcc Cu and bcc Ta crystals.

In addition to the crystal structures indicated above, energies of several 32-atom supercells containing liquid alloys with the CuTa composition have been computed at the potential testing stage. Details of these liquid structures will be explained later (Sec. II D 2).

For testing the chemical binding across Cu-Ta interfaces, the interface energy as a function of separation has also been included in the database. Given that this part of the first-principles data is only needed for testing purposes, and since the high cutoff energy mentioned above would make the calculations with the plane-wave code prohibitively slow, we use the results of previous calculations[14] employing the mixed-basis pseudopotential (MBPP) method.[18–23] These calculations use a supercell composed of five Ta (110) layers followed by seven or eight Cu (111) layers. The layers are oriented according to the Nishiyama-Wasserman orientation relationship: $(111)_{\mathrm{fcc}}\|(110)_{\mathrm{bcc}}$ and $[1\bar{1}0]_{\mathrm{fcc}}\|[001]_{\mathrm{bcc}}$. The Cu layers are stretched in in-plane directions to coherency with Ta. There are four different ways of placing a Cu layer on top of Ta (110), referred to here as "on top," "bridge," "bcc type," and "fcc type" (see Ref. 14 for details). In this work, all four have been tested. After the construction, the supercell has been relaxed by varying its dimension normal to the interface and the spacings between individual Cu layers.

The interface separation process is modeled by varying the interfacial spacing Δ of the adjacent Cu and Ta layers across the interface (by the periodic boundary conditions, the supercell effectively contains two such interfaces, both of which are being separated). In this process, no relaxation is allowed. The separation continues until we end up with isolated Cu and Ta slabs. At each step, the interface binding energy E_{sep} is determined as the energy difference per unit interface area relative to the completely separated state. Thus, $E_{sep}\to 0$ at $\Delta\to\infty$ by definition. The function $E_{sep}(\Delta)$ calculated in this manner characterizes the strength of the bonding across the Cu-Ta interface.

C. Potential parametrization and fitting

The pair-interaction function is chosen in the generalized Morse form,

$$\Phi_{\mathrm{CuTa}}(r)=\psi\left(\frac{r-r_c}{h}\right)[A(e^{-qb(r-r_0)}-qe^{-b(r-r_0)})+\delta], \quad (6)$$

where $\psi(x)$ is a cutoff function defined by

$$\psi(x)=\frac{x^4}{1+x^4} \quad (7)$$

if $x<0$ and $\psi(x)\equiv 0$ if $x\geq 0$. This cutoff function guarantees that $\Phi_{\mathrm{CuTa}}(r)$ and its first three derivatives smoothly turn to zero at a cutoff distance r_c. Equation (6) contains the fitting parameters A, q, b, r_0, δ, r_c, and h. The dipole and quadrupole functions are postulated in the form

$$u_{\mathrm{CuTa}}(r)=\psi\left(\frac{r-r_c}{h}\right)(d_1e^{-d_2r}+d_3), \quad (8)$$

TABLE I. Optimized values of fitting parameters of the ADP Cu-Ta potential.

Parameter	Value
r_c (nm)	0.5579
h (nm)	1.7078
A (eV)	6.6231×10^{-4}
r_0 (nm)	0.4308
b (1/nm)	2.0022×10^{1}
q	1.9496
δ (eV)	1.6649
d_1 ($\mathrm{eV}^{1/2}$/nm)	6.0674
d_2 (1/nm)	−0.7532
d_3 ($\mathrm{eV}^{1/2}$/nm)	−7.3773
q_1 ($\mathrm{eV}^{1/2}/\mathrm{nm}^2$)	5.6243×10^{1}
q_2 (1/nm)	2.5965
q_3 ($\mathrm{eV}^{1/2}/\mathrm{nm}^2$)	-2.4565×10^{1}
s_{Ta}	0.2628
g_{Cu} (eV)	−0.8421
g_{Ta} (eV)	-1.0707×10^{3}

$$w_{\mathrm{CuTa}}(r)=\psi\left(\frac{r-r_c}{h}\right)(q_1e^{-q_2r}+q_3), \quad (9)$$

where q_i and d_i are fitting parameters. Both functions are subject to the same cutoff as $\Phi_{\mathrm{CuTa}}(r)$. Together with the transformation coefficients mentioned above, this parametrization includes 16 fitting parameters.

The parameters have been optimized by minimizing the weighted mean-squared deviation of the ADP binding relations from the respective first-principles binding relations using a simulated annealing method. After the fit, the optimized $\Phi_{\mathrm{CuTa}}(r)$ function has been modified by adding a term $10(r-r_*)^4$ at $r<r_*=0.27$ nm to eliminate an unphysical feature at short atomic separations. The optimized values of the fitting parameters are summarized in Table I and the pair-interaction functions are shown in the effective-pair format[6] in Fig. 1. Tabulated forms of the potential functions are available from the authors on request.

D. Testing the potential

1. Crystal structures

The binding curves for the cubic compounds used in the potential fit are shown in Fig. 2. The agreement between the ADP and first-principles CPMD energies is very reasonable for the $L1_1$ and $L1_2$ structures and excellent for $L1_0$ and $B2$. Overall, given the approximate character of the ADP model, the potential displays good transferability over the entire concentration range.

Table II summarizes the equilibrium formation energies of several compounds obtained by first-principles CPMD and ADP calculations. Note that the first-principles energy of $L1_2$-Cu_3Ta (0.350 eV) compares well with the recent calculation by Gong *et al.* (0.357 eV).[24] The agreement between

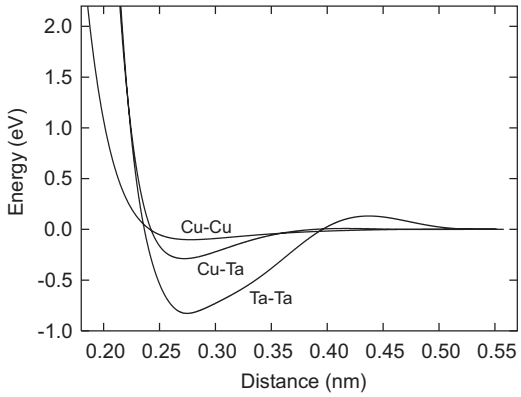

FIG. 1. The pair-interaction functions of the Cu-Ta ADP potential in the effective-pair format.

the ADP and first-principles calculations is good for the cubic compounds and layered structures but less accurate for the C11 compounds. There is notable disparity for the energies of the $C11_f$-Cu_2Ta and $C11_b$-Ta_2Cu compounds both with and without atomic relaxation. It should be emphasized that C11 structures were not included in the potential fit and that this is a very severe test of the potential that involves strong deformations along an extended path in the configuration space. In fact, the Bain path is a rather stringent test even for interatomic potentials for pure metals.

The relaxed impurity formation energies predicted by the potential are 0.962 eV for Cu in Ta and 1.027 eV for Ta in Cu. The corresponding first-principles numbers are 0.463 and 0.836 eV, respectively. These numbers were obtained in small supercells. Note that the impurity data were not included in the potential fit. After relaxation in large simulation blocks, the ADP impurity formation energies become 0.764 eV for Cu in Ta and 1.096 eV for Ta in Cu, which are in good agreement with the first-principles results. These numbers are high enough to secure the experimentally established[13] negligible solid solubility between Cu and Ta.

For the applications intended in this work, it is requisite to have a potential that does not produce any stable Cu-Ta compounds at any composition or temperature. As a check of this property, the potential has been applied to minimize the energies of all compounds listed in Table II with respect to all possible supercell shape variations and local atomic displacements. Although this full relaxation does reduce the formation energy of some of the compounds, it remains always positive. Fully relaxed formation energies of a number of additional compounds have been computed and found to be positive as well, including $B32$-CuTa, $D0_3$-Ta_3Cu, $D0_3$-Cu_3Ta, $D0_{19}$-Ta_3Cu, $D0_{19}$-Cu_3Ta, $D0_{22}$-Ta_3Cu, and $D0_{22}$-Cu_3Ta. Furthermore, extensive semi-grand-canonical Monte Carlo simulations[25] were performed at different temperatures and chemical-potential differences $\Delta\mu=\mu_{Ta}-\mu_{Cu}$

TABLE II. Equilibrium formation energies (in eV per atom, relative to fcc Cu and bcc Ta) of Cu-Ta compounds obtained by first-principles CPMD calculations and with the ADP potential. (♣—no minimum found.)

Structure	*Ab initio*	ADP
	Cubic structures[a]	
$L1_2$-Cu_3Ta	0.350[b]	0.241
$L1_0$-CuTa	0.075[b]	0.091
$L1_1$-CuTa	0.228[b]	0.193
B_2-CuTa	0.139[b]	0.121
$L1_2$-Ta_3Cu	0.126[b]	0.076
	Layered structures[b]	
CuCuTa	0.219	0.172
CuCuCuTaTaTa	0.387[b]	0.351
CuTaTa	0.352	0.294
	C11 structures[c]	
$C11_f$-Cu_2Ta	0.098	0.069
$C11_b$-Cu_2Ta	♣	♣
$C11_f$-Ta_2Cu	0.158	0.090
$C11_b$-Ta_2Cu	0.114	0.030
	C11 structures[d]	
$C11_f$-Cu_2Ta	0.063	0.025
$C11_b$-Cu_2Ta	♣	♣
$C11_f$-Ta_2Cu	0.141	0.087
$C11_b$-Ta_2Cu	0.046	0.022

[a]Volume relaxation only.
[b]Data included in the potential fit.
[c]Relaxation of volume and c/a.
[d]Relaxation of volume, c/a, and atomic positions.

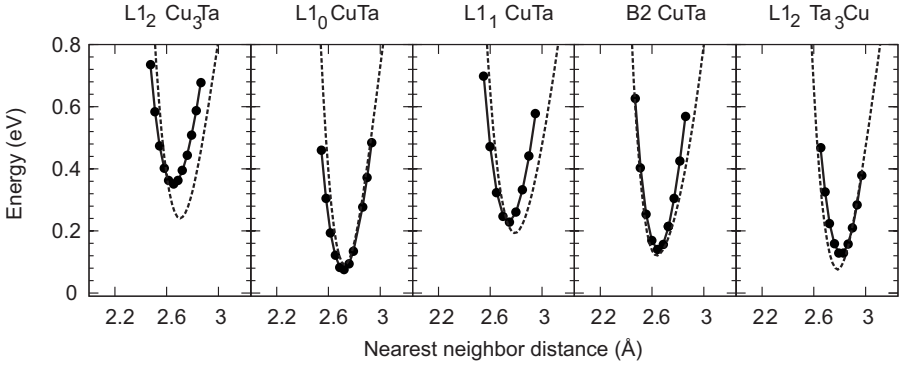

FIG. 2. Formation energy (per atom) versus atomic volume for ordered Cu-Ta compounds used for fitting the ADP potential. Points—first-principles CPMD calculations; dashed lines—ADP results.

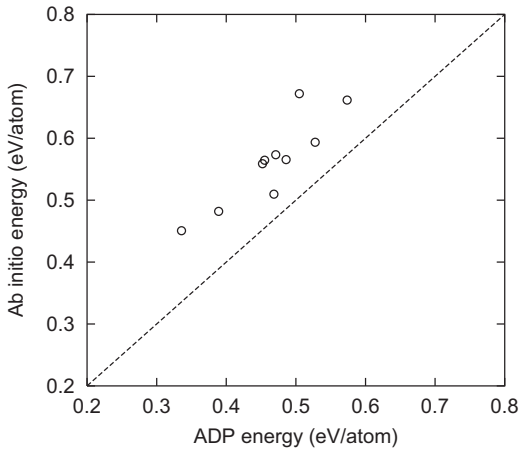

FIG. 3. Formation energies (relative to fcc Cu and bcc Ta) of liquid supercells with the Cu-50 at % Ta composition obtained by first-principles CPMD calculations and with the ADP potential. The line of perfect correlation is shown as a reference. The variation of the energy reflects fluctuations during MD simulations of a 32-atom supercell. The liquid energies were not included in the potential fit.

starting from compositionally disordered configurations. The result was invariably either almost pure Cu or almost pure Ta. No other solid phases were observed in the simulations. Although these tests do not constitute a rigorous proof that no intermediate phases can exist with this potential, they do give reasonable confidence that this will be the case in atomistic simulations.

2. Liquid phase

To test liquid properties, we created a 32-atom supercell of a CuTa compound and heated it up to a high temperature using molecular dynamics (MD) with the potential. After the supercell had melted, it was cooled down to the temperature of 2000 K and equilibrated by running an isothermal-isobaric NPT MD simulation at zero pressure for a few nanoseconds. The simulation was then continued for 10 ns more and a snapshot was saved after each nanosecond. The energies of the ten snapshots thus produced were determined with the ADP potential and by the first-principles methods discussed in Sec. II B.

In Fig. 3, the ADP formation energies of the liquid supercells are plotted against their first-principles counterparts. Although the first-principles numbers are systematically on the higher side of the perfect agreement line, there is a clear correlation between the two calculation methods.

As a further test, the position of the liquidus line on the phase diagram has been explored by semi-grand-canonical Monte Carlo simulations. The methodology was similar to the one recently used in Ref. 26 and involved a solid-liquid interface that can move by consuming one phase or the other, depending on whether the temperature and composition are below or above the liquidus. At a fixed temperature, the chemical-potential difference $\Delta\mu$ can be adjusted to approach the solid and/or liquid equilibrium (no interface motion during a long simulation run). The respective equilibrium phase compositions are then computed by separate runs on single-phase systems at the estimated equilibrium T and $\Delta\mu$ values. In this work, an accurate phase diagram calculation by this method is a computationally extensive procedure and was not pursued. However, a few points have been estimated and found to be in qualitative agreement with the liquidus line on the experimental phase diagram.[13] This is enough to reassure that the potential can adequately represent interactions between liquid Cu and solid Ta. As a side observation, liquid alloys undercooled below the liquidus line underwent a separation into Cu-rich and Ta-rich liquid phases with a well-defined interface. This observation is in encouraging agreement with the kinetic liquid separation line and a critical point shown in the experimental phase diagram.[13]

3. Surface decohesion

In the context of future applications to Cu-Ta interfaces, it is important to verify that the ADP potential provides an adequate description of binding between the Cu and Ta surfaces. In Fig. 4, we compare the interface binding curves obtained on identical supercells by first-principles MBPP cal-

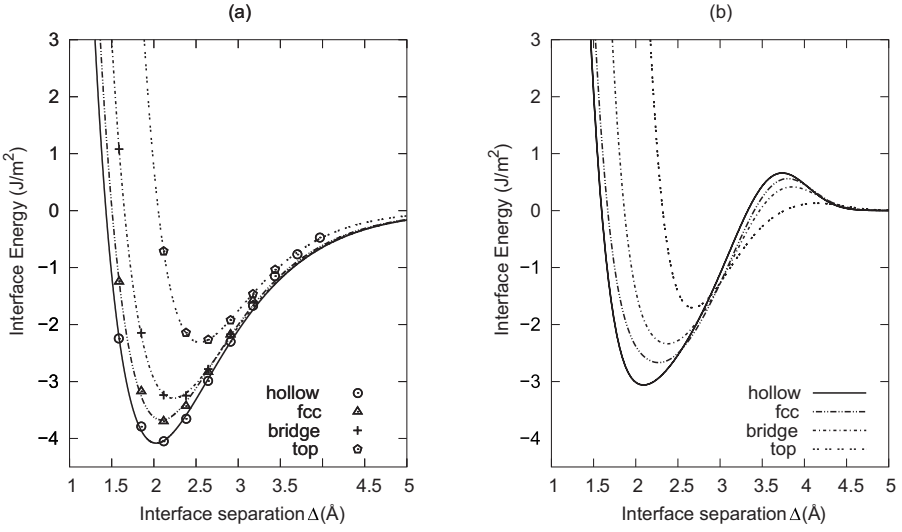

FIG. 4. Binding energy between Cu (111) and Ta (110) surfaces as a function of separation obtained (a) by first-principles MBPP calculations and (b) with the ADP potential. Different curves represent alternate translational states of the Cu-Ta interface.

culations and using the ADP potential. The curves have been computed for four types of relative translations of the adjacent Cu and Ta layers indicated in Sec. II B. The minimum on each curve corresponds to the equilibrium spacing of the Cu and Ta slabs, while its depth gives the equilibrium work of separation W_s.

While the potential tends to underbind the interfaces, the ranking of the W_s values and the equilibrium separations corresponding to the different translational states are correct. The potential produces a hump at separations of about 3.5 Å. This artifact of the potential, apparently arising from an interplay between different shapes of the potential functions, might affect atomistic simulations involving Cu and Ta surfaces separated by this distance. This should be kept in mind in applications of this potential. For interface separations close to equilibrium, however, this hump is unlikely to produce artifacts.

III. APPLICATION TO WETTING AND THIN-FILM STABILITY

To further assess the ability of the ADP potential to reliably reproduce interface properties between Cu and Ta, we have examined the stability and wetting behavior of thin Cu films deposited on a Ta substrate. This has been the subject of several recent experimental and atomistic simulation studies.[8,9,14,27–30] We will limit the discussion to a particular problem for which a controversy exists in the literature, namely, whether Cu completely dewets from a Ta substrate or whether it leaves a monolayer (ML) coverage.[8,14,29,30]

Experimental studies by Kuhn *et al.*[27] have demonstrated that ultrathin Cu films deposited on Ta (110) substrates form a stable two-dimensional film for coverages of up to 1.22 ML, with a mismatch occurring along the $[1\bar{1}0]$ direction of the substrate. Additionally, deposited Cu atoms form three-dimensional (3D) clusters on top of the Cu film. Similar results are reported by Chen *et al.*[28] for Cu deposited on polycrystalline Ta substrates, which also demonstrate that for a submonolayer (2 Å) coverage, a pseudomorphic Cu monolayer is stable both at room temperature and after annealing at a temperature of 1000 K. However, for the coverage of 5 Å and higher, dewetting of Cu from Ta is observed.[28] An instability of Cu films with thicknesses of up to 50 Å deposited on Ta (110) and Ta (100) at room temperature was reported by Venugopal.[31] Upon heating, the films break up and agglomerate into islands, leaving 1 or 2 ML thick Cu films on the substrate. The remaining Cu forms micronsize islands with fcc crystal structure. The (111) planes of Cu are aligned parallel to the substrate surface and satisfy the Nishiyama–Wasserman orientation relationship. On the other hand, Kim *et al.*[29] reported complete dewetting of Cu from Ta with a nonwetting contact angle of $123 \pm 8.5°$ and no evidence of a monolayer coverage. An additional experimental observation has recently been reported by Fillot *et al.*,[30] who found that thin Cu films are indeed unstable and dewet from Ta to form Cu clusters on top of a stable Cu monolayer on both bcc Ta and tetragonal β-Ta substrates.[30]

MD simulations performed by Klaver and Thijsse[7,8] indicate that Cu atoms deposited on Ta (110) or (100) form a stable monolayer film with a "fish-bone" or "rippled" structure, with 3D Cu islands growing on top of it. Upon further deposition, the islands coalesce and form an almost perfect fcc structure. However, no indication of Cu film dewetting has been given in that work. Similar conclusions have been reached in the MD simulations with an EAM Cu-Ta potential by Li and Adams.[9]

Recently, the mechanical and thermodynamic stability of Cu thin films on Ta was investigated by the first-principles MBPP method.[14] It was shown that a monolayer of Cu on Ta (110) should indeed be stable and that excess Cu should dewet from Ta and leave a Cu monolayer on Ta.

In this study, it is not our intention to conduct an atomistic simulation of a "deposition experiment." Instead, we seek to demonstrate that the ADP potential is capable of reproducing the basic features of interaction of Cu films with Ta, particularly the stability of a Cu monolayer on Ta and instability of multilayer films, resulting in their dewetting from the monolayer. To this end, we examine two different initial configurations: (i) thin Cu film placed on a Ta (110) substrate and (ii) liquid Cu drop placed on a Ta (110) surface. In both cases, the evolution of the system is studied by MD at a constant temperature of 1400 K, which is above the melting point of Cu [1327 K (Ref. 11); the experimental value is 1357 K (Ref. 32)] but below that of Ta [3960 K (Ref. 12); the experimental value is 3290 K (Ref. 32)]. The first case should indicate whether a multilayer film is stable, whereas the second case is a test of the wetting behavior of Cu on Ta. The simulations are performed using the ITAP MD software package (IMD).[33]

In the first case, the initial Cu film is composed of two fcc (111) layers placed on the (110) surface of bcc Ta, as shown in Fig. 5(a). The Kurdjumov-Sachs orientation relationship is applied, $(111)_{\mathrm{fcc}} \| (110)_{\mathrm{bcc}}$ and $[0\bar{1}1]_{\mathrm{fcc}} \| [\bar{1}1\bar{1}]_{\mathrm{bcc}}$, which is obtained from the Nishiyama-Wasserman orientation by a 5.26° rotation about the interface normal. The substrate is composed of eight Ta (110) layers, so that the system contains 24 000 Ta atoms and 8064 Cu atoms. The system dimensions parallel to the interface are 14.3×16.2 nm^2, with the initial thickness of 23.12 nm. Periodic boundary conditions are applied parallel and free boundary conditions perpendicular to the interface. The bottom Ta layer is kept fixed throughout the simulation in order to mimic a semi-infinite substrate. After a MD run for about a nanosecond at 1400 K, the system is slowly cooled down to room temperature.

In the MD snapshots shown in Fig. 5, the Ta atoms are represented by the dark-blue color, while the color of the Cu atoms reflects their potential energy according to the energy scale indicated in the figure. During the first 50 ps, the Cu film maintains its integrity across the entire substrate as seen in Fig. 5(b). After about 60 ps, the top Cu layer breaks up and forms a number of voids that expose the underlying Cu layer [Fig. 5(c)]. From the color of the Cu atoms in the top layer, it is evident that they have a higher potential energy than the atoms underneath. As the simulation progresses [Figs. 5(d)–5(g)], the atoms of the top layer agglomerate and form two liquid drops with comparable sizes and shapes. By the time $t=340$ ps, the drops are completely formed and do not practically change for the rest of the simulation, aside

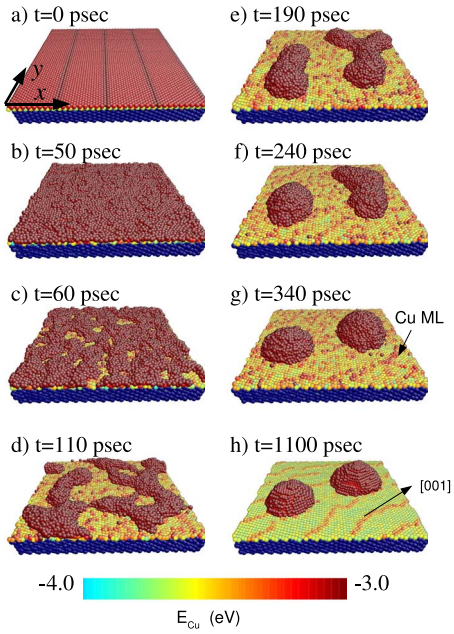

FIG. 5. (Color online) A sequence of snapshots from a molecular dynamics simulation of two fcc Cu (111) layers on a bcc Ta (110) substrate at $T=1400$ K, demonstrating dewetting of the top Cu layer and the formation of two Cu drops. The Ta atoms are represented by a blue color, while the Cu atoms are colored according to their potential energy using the energy scale at the bottom of the figure. The directions indicated by the axes in (a) correspond to the Kurdjumov-Sachs orientation relationship with the lattice directions $[0\bar{1}1]_{\mathrm{fcc}}\|[\bar{1}1\bar{1}]_{\mathrm{bcc}}$ pointing along the x axis and the lattice directions $[2\bar{1}\bar{1}]_{\mathrm{fcc}}\|[\bar{1}12]_{\mathrm{bcc}}$ pointing along the y axis.

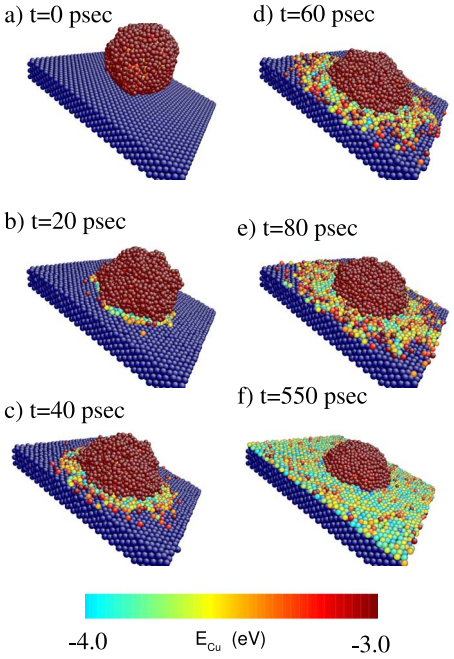

FIG. 6. (Color online) A sequence of snapshots from a molecular dynamics simulation of a Cu drop spreading on a Ta (110) substrate at 1400 K. A monolayer of Cu spreads and a stable wetting drop forms on top of it. The color coding is the same as in Fig. 5.

from slight Brownian movements and small spontaneous rotations. The drops form a wetting angle with the remaining Cu monolayer of approximately 56°. It is expected that, in a much longer MD run, they would eventually coalesce into a single drop.

After cooling down to 300 K, the drops solidify and the underlying monolayer becomes more ordered, as shown in Fig. 5(h). The crystal structure inside the drops is fcc and their shape is faceted. The crystal planes parallel to the facets and to the underlying monolayer are found to be (111). The monolayer consists of regions with coherent, pseudomorphic structure that replicates the structure of the Ta substrate. Such pseudomorphic regions are separated by lines of mismatch, which are aligned approximately parallel to the [001] direction of the Ta substrate. Both the structure of the monolayer and the direction of the misfit lines may depend on the initial condition and the annealing schedule (particularly, the cooling rate). More details regarding the monolayer structure will be published elsewhere. The results displayed in Fig. 5 clearly demonstrate that a bilayer Cu film is unstable and dewets, forming Cu droplets on top of a stable Cu monolayer. Thus, the ADP potential reproduces the instability of thin Cu films experimentally demonstrated.[28,30,31]

In the second case, a liquid Cu drop composed of 3344 atoms and separately equilibrated at 1400 K is brought in contact with a Ta (110) substrate of dimensions 9.92×11.2 nm^2 parallel to the surface, as shown in Fig. 6(a). The surface area of the substrate is chosen so that the number of the Cu atoms in the drop would be sufficient to completely cover the substrate with 1 ML and leave enough atoms to agglomerate on top of it. The thickness of the substrate is the same as in the previous case.

The system is then subject to a MD run at 1400 K for 0.55 ns. Figure 6 shows a series of snapshots from the simulation, with the color coding similar to the previous case. At early stages of the simulation, a "skirt" forms around the drop [Fig. 6(b)], which continues to spread over the Ta substrate until it completely covers it, producing a stable Cu monolayer. The rest of the Cu atoms remain in the drop, which becomes smaller than the initial one. This structure remains stable for the rest of the simulation. The wetting angle between the drop and the monolayer is close to the one found in the previous case. This simulation provides further evidence that a stable Cu monolayer is formed regardless of the initial condition. It further confirms the ability of the ADP potential to reproduce the wetting behavior of Cu on Ta.

IV. CONCLUSIONS

In this work, the angle-dependent Cu-Ta potential developed utilizes existing potentials for pure Cu and Ta, thus focusing on the cross interactions. The cross-interaction functions have been obtained by fitting to first-principles binding relations for a number of crystal structures with different symmetries and chemical compositions. The approach in which a binary potential is produced by fitting cross interactions to first-principles information with only a few experi-

mental numbers, if any, is relatively recent. It essentially turns the potential generation process into a parametrization of first-principles data (see the discussion in Ref. 6) and recent examples of Ni-Al and Cu-Ag potentials.[15,26] This approach is especially justified for the Cu-Ta system, which simply does not contain any intermediate solid phases of the experimental phase diagram. Thus, using first-principles calculations for artificial intermetallic compounds is the only way of generating a potential.

Here, the first-principles database used for both the fitting and testing of the potential has been generated within the density-functional formalism using two different methods: CPMD and MBPP. Besides the energies of several well-known crystal structures, the database includes purely artificial layered structures representing possible atomic arrangements near coherent interfaces. It also includes energy-separation curves for several coherent interfaces, as well as a number of liquid supercells. All together, the database spans a large area of configuration space and presents an ideal testing bed for an interatomic potential.

The tests indicate that the potential is transferable to a wide range of chemical compositions and atomic environments. Some of the physical properties compare well with their first-principles counterparts, while others are less accurately reproduced. Given the complex and highly dissimilar nature of the Cu-Ta system and the semiempirical character of the ADP model, we conclude that the potential is quite suitable for atomistic simulations of this system.

We have applied the potential in MD simulations of Cu wetting and dewetting on a Ta substrate. The simulations show that a Cu film placed on a Ta (110) surface dewets from it but leaves a stable Cu monolayer on the surface. The excess Cu atoms agglomerate into droplets on top of the monolayer, forming a relatively large wetting angle of about 56°. Furthermore, if a droplet of Cu is placed on a clean Ta (110) substrate, exactly 1 ML spreads over the surface, while the excess Cu atoms remain in the droplet. Thus, we clearly observe high stability of a Cu monolayer on Ta and instability of thicker films. This finding is encouragingly consistent with our recent first-principles calculations[14] of thermodynamics and mechanical properties of Cu-Ta interfaces. It is also in good agreement with experimental studies of thermal stability of Cu films deposited on Ta substrates.

This work is part of our ongoing effort to create a fundamental understanding of the structure, thermodynamic stability, and mechanical properties of Cu-Ta interfaces. In this work, the ADP potential developed enables large-scale simulations of such interfaces using MD and other atomistic methods.

ACKNOWLEDGMENTS

Financial support provided by the Deutsche Forschungsgemeinschaft (DFG) through Contract No. Gu367/24-1 is gratefully acknowledged. Y.M. was supported by the U.S. Department of Energy, Office of Basic Energy Sciences.

*adham.hashibon@iwm.fraunhofer.de

[1] K. Holloway, P. M. Fryer, C. Cabral, Jr., J. M. E. Harper, P. J. Bailey, and K. H. Kelleher, J. Appl. Phys. **71**, 5433 (1992).
[2] B.-S. Kang, S.-M. Lee, J. S. Kwak, D.-S. Yoon, and H. K. Baik, J. Electrochem. Soc. **144**, 1807 (1997).
[3] T. Laurila, K. Zeng, J. K. Kivilahti, J. Molarius, and I. Suni, J. Appl. Phys. **88**, 3377 (2000).
[4] M. Stavrev, D. Fischer, F. Praessler, C. Wenzel, and K. Drescher, J. Vac. Sci. Technol. A **17**, 993 (1999).
[5] M. S. Daw and M. I. Baskes, Phys. Rev. B **29**, 6443 (1984).
[6] Y. Mishin, in *Handbook of Materials Modeling*, edited by S. Yip (Springer, Dordrecht, The Netherlands, 2005), Chap. 2.2, pp. 459–478.
[7] P. Klaver and B. Thijsse, *Magnetic and Electronic Films—Microstructure, Texture and Application to Data Storage*, MRS Symposia Proceedings No. 721 (Materials Research Society, Pittsburgh, 2002), p. J2.3.1.
[8] P. Klaver and B. Thijsse, J. Comput.-Aided Mater. Des. **10**, 61 (2003).
[9] Y. Li and J. B. Adams, *Magnetic and Electronic Films—Microstructure, Texture and Application to Data Storage*, MRS Symposia Proceedings No. 721 (Materials Research Society, Pittsburgh, 2002), p. J3.7.1.
[10] Y. Mishin, M. J. Mehl, and D. A. Papaconstantopoulos, Acta Mater. **53**, 4029 (2005).
[11] Y. Mishin, M. J. Mehl, D. A. Papaconstantopoulos, A. F. Voter, and J. D. Kress, Phys. Rev. B **63**, 224106 (2001).
[12] Y. Mishin and A. Y. Lozovoi, Acta Mater. **54**, 5013 (2006).
[13] *Binary Alloy Phase Diagrams*, edited by T. B. Massalski (ASM, Materials Park, OH, 1986).
[14] A. Hashibon, C. Elsässer, Y. Mishin, and P. Gumbsch, Phys. Rev. B **76**, 245434 (2007).
[15] Y. Mishin, Acta Mater. **52**, 1451 (2004).
[16] J. Hutter, A. Alavi, T. Deutsch, and M. Parrinello, CPMD Version 3.3, MPI, Stuttgart and IBM Research Laboratory, Zürich.
[17] A detailed crystallographic description of these and other structures studied in this work can be found at http://cst-www.nrl.navy.mil/lattice/
[18] C. L. Fu and K. M. Ho, Phys. Rev. B **28**, 5480 (1983).
[19] C. Elsässer, N. Takeuchi, K. M. Ho, C. T. Chan, P. Braun, and M. Fähnle, J. Phys.: Condens. Matter **2**, 4371 (1990).
[20] K. M. Ho, C. Elsässer, C. T. Chan, and M. Fähnle, J. Phys.: Condens. Matter **4**, 5189 (1992).
[21] F. Lechermann, F. Welsch, C. Elsässer, C. Ederer, M. Fähnle, J. M. Sanchez, and B. Meyer, Phys. Rev. B **65**, 132104 (2002).
[22] F. Lechermann, M. Fähnle, B. Meyer, and C. Elsässer, Phys. Rev. B **69**, 165116 (2004).
[23] B. Meyer, C. Elsässer, F. Lechermann, and M. Fähnle, FORTRAN90, program for mixed-basis pseudopotential calculations for crystals, Max-Planck-Institut für Metallforschung, Stuttgart.
[24] H. R. Gong, L. T. Kong, W. S. Lai, and B. X. Liu, Acta Mater. **51**, 3885 (2003).
[25] D. Frenkel and B. Smit, *Understanding Molecular Simulation* (Academic, San Diego, 2002).

[26] P. L. Williams, Y. Mishin, and J. C. Hamilton, Modell. Simul. Mater. Sci. Eng. **14**, 817 (2006).
[27] W. K. Kuhn, R. A. Campbell, and D. W. Goodman, J. Phys. Chem. **97**, 446 (1993).
[28] L. Chen, N. Magtoto, B. Ekstrom, and J. Kelber, Thin Solid Films **376**, 115 (2000).
[29] H. Kim, T. Koseki, T. Ohba, T. Ohta, Y. Kojima, H. Sato, and Y. Shimogaki, J. Electrochem. Soc. **152**, G594 (2005).
[30] F. Fillot, Z. Tokei, and G. Beyer, Surf. Sci. **601**, 986 (2007).
[31] V. Venugopal, Ph.D. thesis, Technische Universiteit Delft, 2005.
[32] *Handbook of Chemistry and Physics*, edited by R. C. Weast (CRC, Boca Raton, FL, 1984).
[33] J. Stadler, R. Mikulla, and H. Trebin, Int. J. Mod. Phys. C **8**, 1131 (1997).